sustainability

MDPI

Article

Trends in Vegetation Seasonality in the Iberian Peninsula: Spatiotemporal Analysis Using AVHRR-NDVI Data (1982–2023)

Oliver Gutiérrez-Hernández [1,*] and Luis V. García [2]

[1] Department of Geography, University of Málaga (UMA), 29071 Málaga, Spain
[2] Institute of Natural Resources and Agrobiology of Seville (IRNAS), Spanish National Research Council (CSIC), 41012 Seville, Spain; lv.garcia@csic.es
* Correspondence: olivergh@uma.es

Abstract: Vegetation seasonality is a critical indicator of ecological responses to global climate change, especially in the Iberian Peninsula, where the intersection of human activity and climate variability amplifies these effects. Understanding these changes is vital for adopting ecogeographical sustainability and developing effective climate adaptation strategies. This study examines trends in vegetation seasonality in the Iberian Peninsula from 1982 to 2023, based on weekly AVHRR NDVI data (2184 images). By integrating Seasonal Trend Analysis (STA) with Robust Trend Analysis (RTA)—including the Theil–Sen (TS) slope estimator, the Contextual Mann–Kendall (CMK) test ($\alpha = 0.05$), and false discovery rate (FDR) control—we identified significant phenological shifts and widespread vegetation greening. The results reveal a regional response to global patterns of climate change, with 94.2% of the study area exhibiting significant trends, particularly in the Mediterranean ecoregion, where earlier growing seasons are becoming increasingly common. These shifts highlight the urgent need for sustainable land and resource management in the face of accelerating global change. Our findings provide critical insights into the ecological dynamics of the Iberian Peninsula, offering a robust foundation for formulating policies that promote environmental sustainability and enhance resilience to climate change.

Keywords: environmental remote sensing; land surface phenology (LSP); global change; phenological shifts; vegetation greening; climate adaptation strategies; ecogeographical sustainability

Citation: Gutiérrez-Hernández, O.; García, L.V. Trends in Vegetation Seasonality in the Iberian Peninsula: Spatiotemporal Analysis Using AVHRR-NDVI Data (1982–2023). *Sustainability* **2024**, *16*, 9389. https://doi.org/10.3390/su16219389

Academic Editors: Xinchang Zhang, Ying Sun and Yongjian Ruan

Received: 6 August 2024
Revised: 15 October 2024
Accepted: 24 October 2024
Published: 29 October 2024

1. Introduction

One of the most evident impacts of climate change is the alteration of the seasonality trends of vegetation [1]. These temporal shifts are particularly pronounced in the Northern Hemisphere, where the arrival of spring occurs earlier [2–4] and the timing of autumn is undergoing complex changes due to climate change [5,6]. Understanding these shifts is crucial for the sustainable management of ecosystems, as they directly impact natural resource availability and regional-scale management [7].

Traditionally, monitoring vegetation seasonality required meticulous yearly documentation, recorded by hand in notebooks [8]. Modern phenology began in 1736 with Robert Marsham's work *Indications of Spring*. Over the following 62 years, Marsham systematically documented 27 natural phenomena and collected information on 20 species of animals and plants in Norfolk [9]. Today, satellite data are crucial for tracking these changes, estimating vegetation dynamics and trends, assessing vigour or decline, and identifying seasonal shifts [10–13].

Phenology explores plants' and animals' periodic life cycle events and their response to seasonal and interannual climate variations [14]. Land surface phenology (LSP) studies vegetation phenology at various scales using data from spaceborne optical sensors [15]. Remote sensing offers significant advantages for phenological studies, including continuously capturing phenological patterns across landscapes and retrospectively analysing phenological data from satellite archives [16].

Phenological metrics focus on critical biological events' timing [17,18]. These metrics are valuable for planning agricultural activities [19], pest management [20], and conducting ecological studies [21]. However, there has been significant variability in the methods used to measure these parameters [22–25]. As a result, the reported findings on phenological trends have shown considerable inconsistency [26]. Given the difficulty of identifying specific phenological events with remotely sensed imagery, the seasonal trend analysis (STA) was developed to describe seasonal curves rather than to identify individual events during their development [27]. This approach primarily focuses on detecting trends in their transformation based on amplitude and phase characteristics from signal processing and time series analysis.

Vegetation indices are essential for studying vegetation dynamics and land surface phenology (LSP) [28]. The most used is the normalised difference vegetation index (NDVI) [29]. In remote sensing, "vegetation dynamics" refers to the spatiotemporal monitoring of the spectral behaviour of vegetation on the Earth's surface [30]. These dynamics, closely linked to phenology, can be influenced by environmental factors (e.g., climate) and human activities (e.g., management practices). Studying vegetation through these indices helps detect environmental trends and changes [31]. Monitoring the Earth's surface using satellite images is a highly active geoscience research area, thanks to abundant open data from international observation programmes [32].

The Mediterranean region is a mosaic of landscapes long affected by human influence, and climate change has now questioned its resilience [33]. The temperature in Mediterranean climate-type regions has increased more rapidly than the global mean rates [34]. Therefore, under the research hypothesis suggesting trends in seasonality, our objective is to analyse trends in vegetation seasonality in the Iberian Peninsula using weekly NDVI composites derived from AVHRR data covering the period from 1982 to 2023.

2. Materials and Methods

2.1. Study Area

The study area is the Iberian Peninsula (Figure 1). Located in the southwestern part of Eurasia, the Iberian Peninsula includes Spain and Portugal, along with the small mountainous country of Andorra and the tiny site of Gibraltar. It is bordered by the Mediterranean Sea to the south and east, the Atlantic Ocean to the west and northwest, and the Pyrenees mountains to the north, which form a natural barrier to France [35,36].

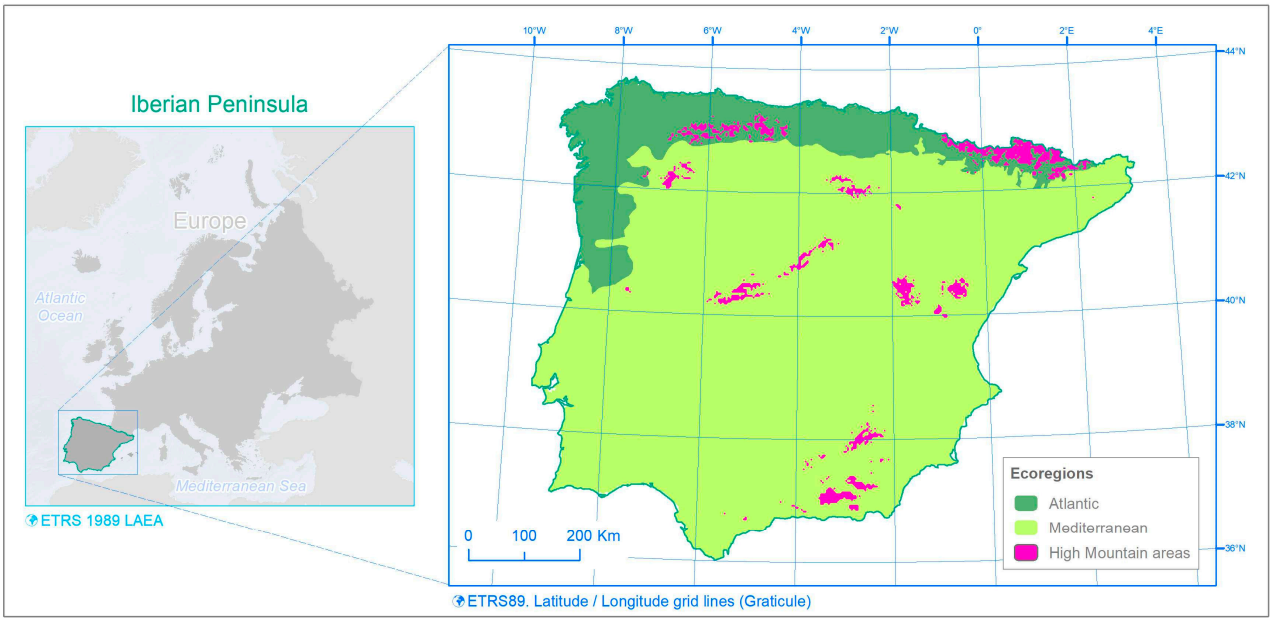

Figure 1. Study area: The Iberian Peninsula. Source: Figure created by the authors.

According to the terrestrial ecoregions of the world [37], the Iberian Peninsula features two major biomes or ecoregions: the Temperate Broadleaf and Mixed Forests and the Mediterranean Forests, Woodlands, and Scrub. The Köppen climate classification [38] associates the Temperate Broadleaf and Mixed Forests biome with the northwest's Oceanic climate (Cfb), characterised by mild temperatures and consistent rainfall. The Mediterranean Forests, Woodlands, and Scrub biome align with the Mediterranean climate (Csa, Csb), featuring hot, dry summers and mild, wet winters.

The Atlantic ecoregion (which includes the Cantabrian and Pyrenean ranges), situated in the northernmost fringe, experiences a notable seasonal contrast, with constant humidity enabling growth during spring and summer and leaf fall in the dense deciduous forests in autumn [39]. Despite the poor soil quality, the high productivity of the vegetation allows forestry and pastoral uses to predominate in this region.

The Mediterranean ecoregion, which covers most of the peninsula, is characterised by a phenology marked by the limiting combination of intense summer heat and drought, restricting growth during the summer [40]. In contrast, spring and autumn are favourable seasons due to mild temperatures and precipitation, promoting budding and flowering. Land use in the Mediterranean region is more complex, with mosaics of agricultural, pastoral, and forestry uses depending on lithology and the availability of water [41].

The High Mountain areas in both ecoregions introduce additional phenological modifications, with longer winters and a brief but intense summer biological activity period [42]. Higher elevations, such as the Pyrenees, Sierra Nevada, Cantabrian Range, and Iberian Range, often experience Continental climates, which can include both non-dry-summer (Df) and dry-summer (Ds) variants [43], characterised by cold winters and significant snowfall. Alpine climates (ETs) are found locally, particularly in the Pyrenees.

2.2. Remote Sensing Data and Preprocessing

We used the smoothed normalised difference vegetation index (SMN) data from the vegetation health products (VHPs) provided by NOAA's Center for Satellite Applications and Research (STAR) [44]. These datasets are derived exclusively from the advanced very-high-resolution radiometer (AVHRR) sensor onboard NOAA's polar-orbiting satellites, covering the period from 1981 to the present. The data are in global area coverage (GAC) format, with a weekly temporal resolution and a spatial resolution of 4 km.

The normalised difference vegetation index (NDVI) values are calculated from surface reflectance data that have been atmospherically corrected to ensure consistency and reliability throughout the entire time series. The SMN dataset is further smoothed to remove cloud contamination and adjusted using the empirical distribution function (EDF) statistical technique. This process corrects sensor degradation, addresses satellite orbital drift, and mitigates the effects of aerosols, significantly improving the overall quality of the data [45].

The SMN data consists of weekly composites of seven Julian days, starting on Thursday and ending on Wednesday, amounting to approximately 52 weeks per year. Our research focused on the period from 1982 to 2023, as the seasonal trend analysis requires data with a complete annual cycle. We worked with 2184 images, corresponding to 52 weekly images per year over 42 years. The dataset includes five weekly gaps due to AVHRR platform issues or other measurement errors [46,47]. To enhance temporal aggregation, we created monthly composites using the maximum value composite NDVI rule [48], ensuring that each month's most significant NDVI value was selected. Additionally, we applied two interpolation methods to address missing or incorrect pixel values and to fill in gaps in our dataset to achieve a complete and curated series: linear temporal interpolation was used to fill in missing images, and harmonic interpolation was used to correct erroneous pixel values by fitting a harmonic regression [49]. These adjustments and corrections ensure the consistency and reliability of the dataset over the study period.

The AVHRR NDVI SMN data are available at a spatial resolution of approximately 4 km. More specifically [50], at the Equator, each pixel measures approximately 4 km per side, resulting in an area of 16 km^2, whereas, for the Iberian Peninsula, the pixel size

is approximately 4.006 km × 3.071 km, resulting in an area per pixel of approximately 12.3 km^2. We applied a data mask of 47,635 pixels (≈586,000 km^2) to focus our analysis on the Iberian Peninsula, which serves as the operational study area. This allowed us to concentrate exclusively on the relevant geographic region and control the scope of multiple testing [51], as each trend test was applied to each pixel.

2.3. Seasonal Trend Analysis (STA) with False Discovery Rate (FDR) Control

We applied seasonal trend analysis (STA), a sequential analytical technique developed by Clark Labs for the Earth Trend Modeller system included in the Terrset 2020 Version 19.0.8 software [27,52]. STA performs a seasonal trend analysis of time series images by calculating trends in seasonal parameters. This procedure uses a two-stage time series analysis to perform a harmonic regression of yearly images, followed by a trend analysis of the amplitude and phases of each year generated by the harmonic regression [27]. Additionally, we incorporated an extra step into the original procedure to control for the false discovery rate (FDR) [53]. Finally, we generated the seasonal curves based on pixels with statistically significant trends, corrected using FDR, ensuring that the visualised trends were robust and reliable.

2.3.1. Modelling Seasonal Parameters

In the first stage, harmonic regression is applied to each yearly time series file using its associated Julian date. The harmonic regression, combined with the inclusion of the Julian date, is preferred over the traditional Fourier method because it accounts for the exact calendar dates of the images, thus producing more reliable results. Harmonic regression is like Fourier analysis, but allows for the specification of Julian dates. Two frequencies are used in harmonic regression to capture the dominant trends in the data without including high-frequency noise [27].

$$y = \alpha_0 + \sum_{n=1}^{n=2} \left\{ a_n \sin\left(\frac{2\pi n t}{T}\right) + b_n \cos\left(\frac{2\pi n t}{T}\right) \right\} + e$$

where α_0 is the mean of the series; a_n and b_n: these are the coefficients of the sinusoidal and cosinusoidal terms, respectively; and n is a harmonic (an integer multiple of the fundamental frequency). Harmonics allow the series to be decomposed into components of different frequencies. In this formula, n ranges from 1 to 2, meaning that the first two harmonics are being considered; t: represents time; T: represents the length of the period; and e represents the error term.

After solving the harmonic regression and rearranging the terms, ignoring the error term, the generalised seasonal curve can be expressed as:

$$y = \alpha_0 + \sum_{n=1}^{n=2} \alpha_n \sin\left(\frac{2\pi n t}{T} + \varphi_n\right)$$

where a_n are the amplitudes for each harmonic, indicating the strength of the annual and semi-annual cycles; and φ_n is the phase shift (ranging from 0° to 360°) for each harmonic, determining the timing of the peaks and troughs of the cycles.

Each annual dataset undergoes harmonic regression to calculate the following shape parameters at the pixel level [54]: amplitude 0 (baseline NDVI level), amplitude 1 (annual cycle strength), amplitude 2 (semi-annual cycle strength), phase 1 (annual cycle start), and phase 2 (semi-annual cycle start). These five parameters can describe a wide range of seasonal curves. Using only two harmonics and the mean, high-frequency noise and variability are rejected. In practice, the most informative seasonality parameter is Amplitude 0, mainly when combined with the other parameters.

2.3.2. Spatiotemporal Trend Analysis

In the second stage, a Theil–Sen (TS) median trend analysis is applied to the five shape parameters over the entire series duration [55,56]. This method, which can handle data with up to 29% outliers, focuses on long-term trends while rejecting short-term variability and noise. We also applied the Contextual Mann–Kendall (CMK) test to compute significance tests on the seasonal trend analysis results [57]. Unlike the original Mann–Kendall test [58,59], the CMK test uses contextual information (first-order eight neighbours) to correct for spatial correlation while also addressing cross-correlation.

The TS slope estimator calculates the median slope from all possible pairwise comparisons of observation values, resulting in a total of N slopes, where $N = \frac{n(n-1)}{2}$. This non-parametric technique for estimating the magnitude of trends in time series data was introduced by Theil (1950) [55] and later refined by Sen (1968) [56]. The equation used to estimate TS slope and intercept are:

$$\text{TS Slope} = \text{Median}\left(\frac{X_j - X_i}{t_j - t_i}\right)$$

$$\text{Intercept} = X_i - \text{MedianSlope} * t_i, \quad \text{for } i = 1 \ldots n$$

where $X_j - X_i$ is the difference in the observation values between two points in time; $t_j - t_i$ is the difference in time between two observations, with t_j being later than t_i; and, here, N represents the total number of non-zero differences $t_j - t_i$ for all pairs (i, j) such that $1 \leq i < j \leq n$. i and j are indices that iterate through the data series, ensuring that i is always less than j, so that all possible pairs of observations are considered without repetition or reversing the order. This is necessary to calculate the slope differences between each pair of observations in the TS method.

This approach offers several advantages. The TS technique is robust to outliers, enabling it to ignore extreme values without affecting the overall slope estimation. It can reject up to approximately 29% of the sample size as outliers (known as the breakdown bound: $1 - \frac{1}{\sqrt{2}} \approx 29.3\%$) without compromising the results, as described in [60].

A widely used method is the MK test to assess the significance of the TS slope [58,59]. Like the TS approach, the MK test evaluates the slopes between all possible pairs of data points. In the MK test, the data are ordered chronologically, with each data point serving as a reference for the subsequent data points in time. The statistic S, introduced by Kendall (1975) [59], is defined as follows:

$$S = \sum_{i=1}^{n-1} \sum_{j=i+1}^{n} \text{sign}(x_i - x_j)$$

where:

$$\text{sign}(\mathrm{x_j} - \mathrm{x_i}) = \begin{cases} 1 \ if \ x_j - x_i > 0 \\ 0 \ if \ x_j - x_i = 0 \\ -1 \, if \ x_j - x_i < 0 \end{cases}$$

and S is the MK test statistic that sums the signs of all differences between pairs of observations; n represents the number of observations in the time series; and $x_i - x_j$ are the values of the time series at time points i and j, respectively. In the MK test, the sign function is used to evaluate whether the difference between two values in a time series is positive, negative, or zero.

The variance σ^2 of S is used to normalise the statistic and is calculated as:

$$\sigma^2 = \frac{n(n-1)(2n+5)}{18} - \sum_{t=1}^{g} \frac{t(t-1)(2t+5)}{18}$$

where σ^2 is the variance of the statistic S; g is the number of tied groups in the dataset; and t represents the size of each tied group. The first term ($\sigma^2 = \frac{n(n-1)(2n+5)}{18}$) accounts for the total variance, while the second term ($\sum_{t=1}^{g} \frac{t(t-1)(2t+5)}{18}$) corrects for ties in the data.

The Z statistic is used to determine the significance of the trend:

$$Z = \begin{cases} \frac{S-1}{\sigma} \; if \; S > 0 \\ 0 \quad if \; S = 0 \\ \frac{S+1}{\sigma} \; if \; S < 0 \end{cases}$$

and:

$$p = 2 \times \Phi(-|Z|)$$

where Z is the standardised test statistic, which follows a normal distribution; p is the p-value, the probability that measures the evidence against the null hypothesis; and Φ represents the cumulative distribution function (CDF) of the standard normal distribution. The value of Z indicates the strength and direction of the trend. If Z is positive and significant, there is an increasing trend; if negative and significant, there is a decreasing trend.

We used the CMK test, an enhanced version of the traditional MK test, to assess the statistical significance of trends in the seasonality parameters [57]. Unlike the original MK test [58,59], the CMK test sequentially incorporates contextual information from first-order eight neighbours to correct for spatial and cross-correlation. The equations used to estimate CMK significance are:

$$Z_m = \frac{\overline{S}_m - E(\overline{S}_m)}{\frac{\sigma}{\sqrt{m}}}$$

and:

$$\overline{S}_m = \frac{1}{m} \sum_{j=1}^{m} S_j$$

and:

$$Var(\overline{S}_m) = \frac{n(n-1)(2n+5)}{18m} = \frac{\sigma^2}{m}$$

where S_j is Kendall's for the j-th neighbour; m = 9 pixels, which includes eight neighbours with central pixel; and $E(S)$ and σ are the mean (expected value) and standard deviation.

Adjustment for cross-correlation is achieved by introducing a covariance term in the calculation of variance:

$$Var(\overline{S}_m) = \frac{1}{m^2} \left[\sum_{j=1}^{m} Var(S_j) + 2 \sum_{j=1}^{m} \sum_{l=1}^{m-j} Cov\left(S_j, S_{j+l}\right) \right]$$

According to Neeti and Ronald Eastman (2014) [57], the CMK method reduces the detection of spurious trends while increasing confidence in the presence of consistent ones. Furthermore, applying the TS slope offers the distinct advantage of filtering out inter-annual variability shorter than 0.29 times the length of the series. Together, these techniques are non-parametric and robust against the influence of outliers.

2.3.3. False Discovery Rate (FDR) Control

Furthermore, we adjusted the p-values from the CMK test using the false discovery rate (FDR) control to account for multiple testing [61], which is an addition to the original procedure to reject false discoveries. Therefore, we only presented the significant trends

($\alpha = 0.05$) in vegetation seasonality of the AVHRR NDVI data based on the CMK test and adjusted with FDR.

The FDR procedure aims to control the proportion of spurious significances (false discoveries) concerning the total number of discoveries (i.e., the total number of tests declared significant) in a multiple-testing context.

Benjamini and Hochberg (BH) introduced the original FDR approach, which is the expected number of false discoveries within all discoveries [62].

The FDR is formally defined as:

$$\mathrm{FDR} = E\left[\frac{V}{R}\right]$$

where E denotes the expected value; V is the number of false positives (false discoveries); and R is the total number of rejected hypotheses (discoveries).

The FDR-BH procedure is applied as follows:

1. Order the p-values of all the hypothesis tests in ascending order:

$$p_{(1)}, p_{(2)}, \ldots, p_{(m)}$$

where $p_{(1)}$ represents the smallest p-value from the set of hypothesis tests; $p_{(2)}$ represents the second smallest p-value; $p_{(m)}$ represents the largest p-value; and m is the total number of hypothesis tests performed.

2. Determine the critical value k as the largest i such that:

$$p_{(i)} \leq \frac{i}{m} \cdot \alpha$$

where $p_{(i)}$ denotes the smallest p-value from the set of hypothesis tests; i is the rank of the p-value when ordered from smallest to largest; i is the total number of hypothesis tests being performed; and α is the desired FDR level.

3. Reject all null hypotheses:

$$H_{(1)}, H_{(2)}, \ldots, H_{(k)}$$

where $H_{(1)}$ represents the hypothesis corresponding to the smallest p-value; $H_{(2)}$ represents the hypothesis corresponding to the second smallest p-value; $H_{(k)}$ represents the hypothesis corresponding to the k-smallest p-value; and, k is the largest rank for which the p-value meets the FDR-BH criterion.

2.3.4. Mapping Trends in Seasonality Parameters and Generalised Seasonal Curves

Our seasonal trend analysis (STA) workflow (Figure 2) applies harmonic regression to model the seasonal parameters of the NDVI data, followed by TS slope estimator and the CMK test to detect significant spatiotemporal trends. To ensure the statistical reliability of the results, we applied the FDR control for multiple testing. This process allowed us to generate detailed maps of seasonality parameters and fit generalised seasonal curves, providing a comprehensive summary of the long-term vegetation dynamics across the study regions.

We generated maps for all five seasonality parameters: amplitude 0 (baseline NDVI level), amplitude 1 (annual cycle strength), amplitude 2 (semi-annual cycle strength), phase 1 (annual cycle start), and phase 2 (semi-annual cycle start). These maps only display statistically significant trends, with the significance levels corrected using the FDR control, ensuring that only robust trends are represented.

To better understand phenological patterns, we fitted and plotted seasonal curves for the Atlantic and Mediterranean ecoregions and High Mountain areas (above 1500 m). These modelled curves represent the start and end of the series, based on the intercepts and slopes of five harmonic shape parameters [63]. Rather than using data from specific years, such as 1982 and 2023, these curves are the best-fit models derived from the entire 42-year

dataset. This generalised approach maximises the use of spatial and temporal information, intentionally excluding short-term variability.

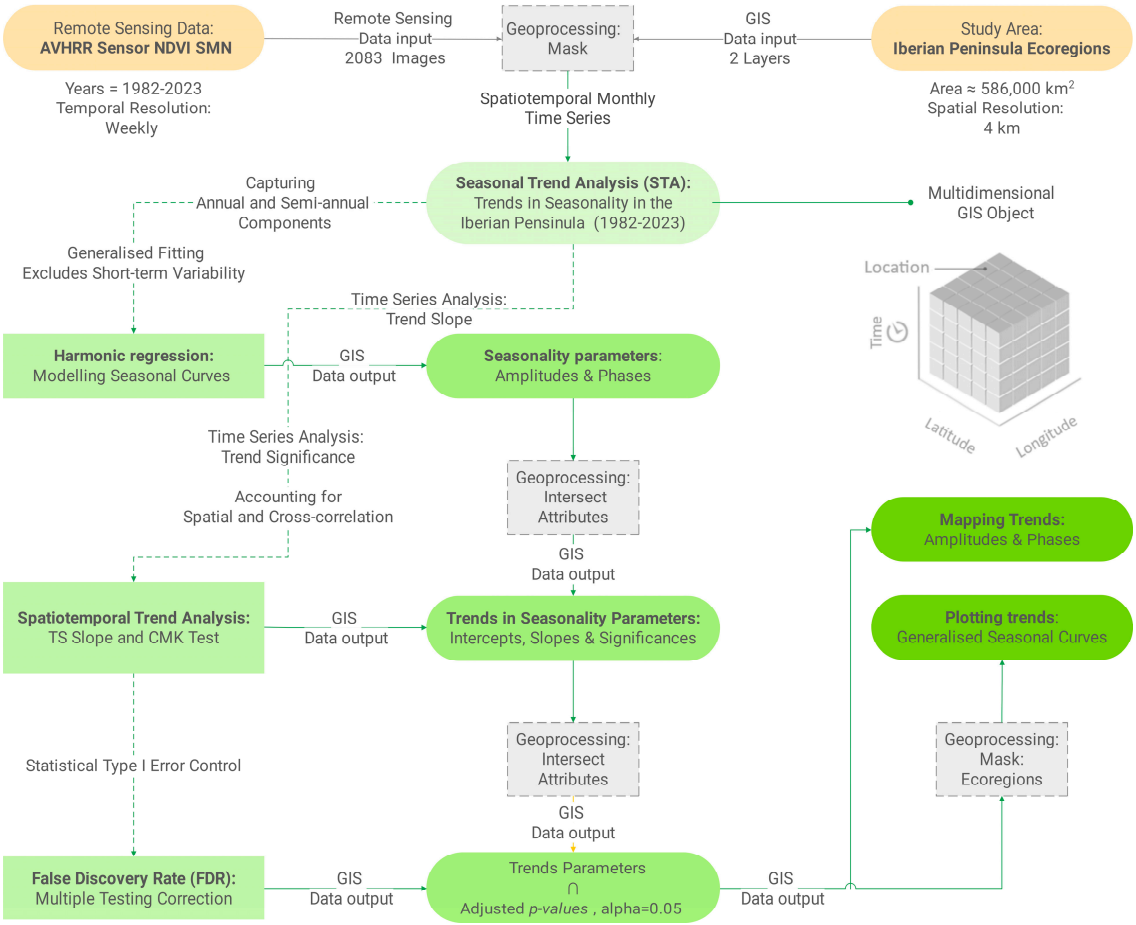

Figure 2. Research workflow diagram for seasonal trend analysis (STA). Source: Figure created by the authors.

The start and end curves are generalised by calculating the median values of the seasonal parameters (amplitude and phase) across all pixels. This includes the mean, annual, and semi-annual cycles. A representative curve summarises the region's overall behaviour using the median slopes and intercepts. This method reduces the impact of outliers and provides a robust, stable depiction of seasonal trends. These idealised curves clearly visualise how seasonal characteristics, such as growth peaks or season onset, have evolved over time, without the influence of short-term noise or variability.

3. Results

Figure 3 shows the spatiotemporal trends of NDVI seasonality parameters (amplitudes and phases) in the Iberian Peninsula from 1982 to 2023.

Among all the seasonality parameters, the most widespread significant trends were observed in amplitude 0 (Figure 3A), with 83.16% of the Iberian Peninsula showing a significant trend in this parameter. Meanwhile, amplitude 1 (Figure 3B), amplitude 2 (Figure 3C), phase 1 (Figure 3D), and phase 2 (Figure 3E) exhibited significant trends in 34.68%, 29.68%, 21.42%, and 20.52% of the area, respectively.

Approximately 94.2% of the Iberian Peninsula experienced a significant trend related to a seasonal parameter for 1982–2023. Within this, about 67.6% of the map showed overlapping significant trends in two to three classes, with the most significant overlap occurring in areas where two (33.0%) and three (34.5%) classes intersected (Figure 3F).

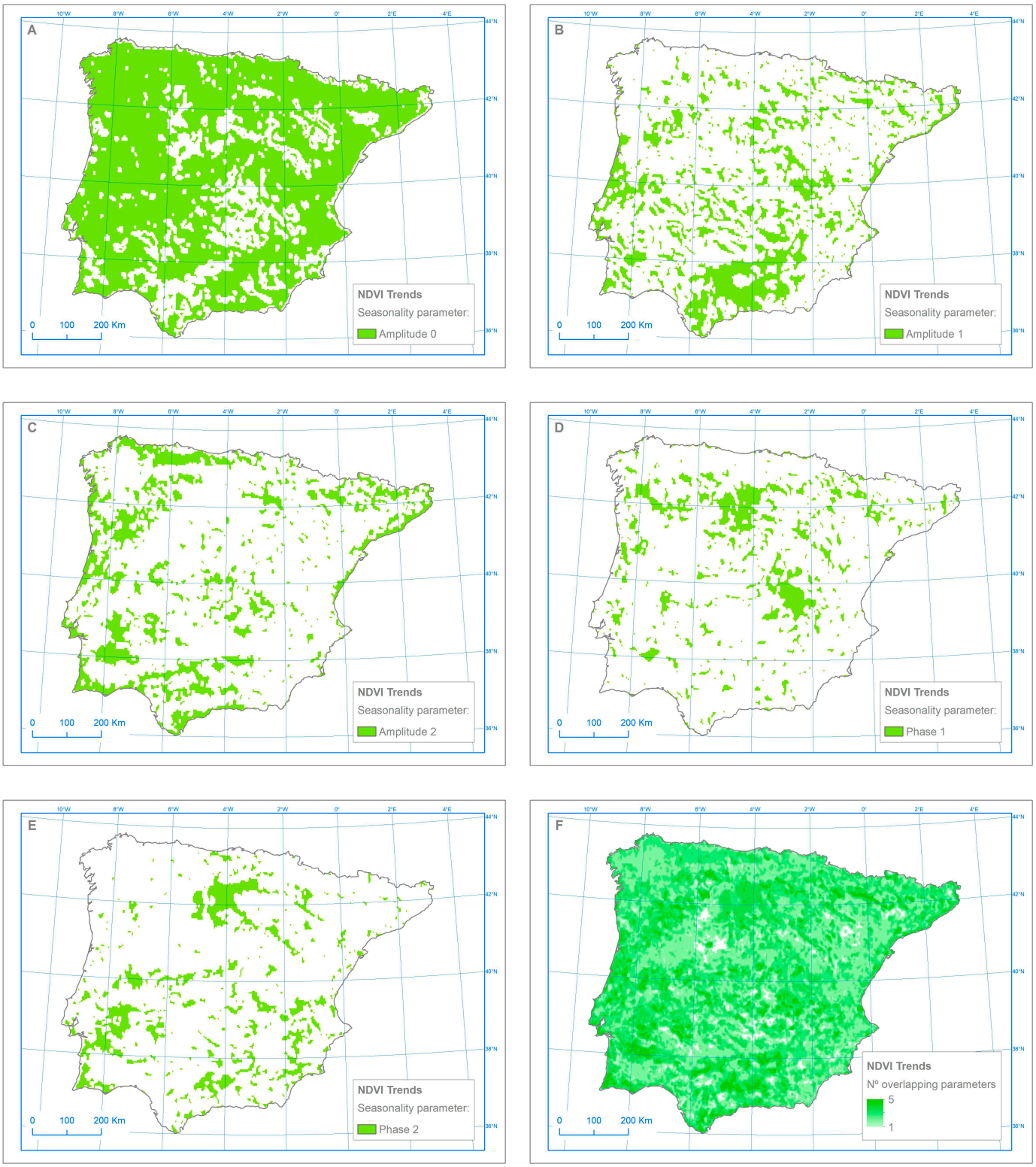

Figure 3. NDVI trends of seasonality parameters in the Iberian Peninsula (1982–2023). Note: Each of the five seasonality parameters was evaluated for trends individually, with binary maps showing whether a trend is present. (**A**) amplitude 0; (**B**) amplitude 1; (**C**) amplitude 2; (**D**) phase 1; (**E**) phase 2; (**F**) The final combined map is also shown, summarising the seasonality parameters with values ranging from 1 to 5. Only the NDVI trends that were statistically significant ($\alpha = 0.05$) using the CMK test with FDR control are shown on the map. Source: Figure created by the authors.

The NDVI baseline (amplitude 0: annual mean) trend showed a positive slope over 95% of the area with significant trends with the FDR control, indicating that greening vegetation was the dominant trend in the Iberian Peninsula from 1982–2023 (Figure 4). The reliability of these trends is further supported by the FDR control applied during the analysis (Figure 5). Before the FDR control, 83.92% of the pixels were identified as significant. After using the FDR control, 83.16% remained significant, with only 0.76% of the pixels classified as false discoveries. This minimal reduction in significant pixels demonstrates the robustness of the detected trends, ensuring that multiple testing errors do not influence the observed greening patterns.

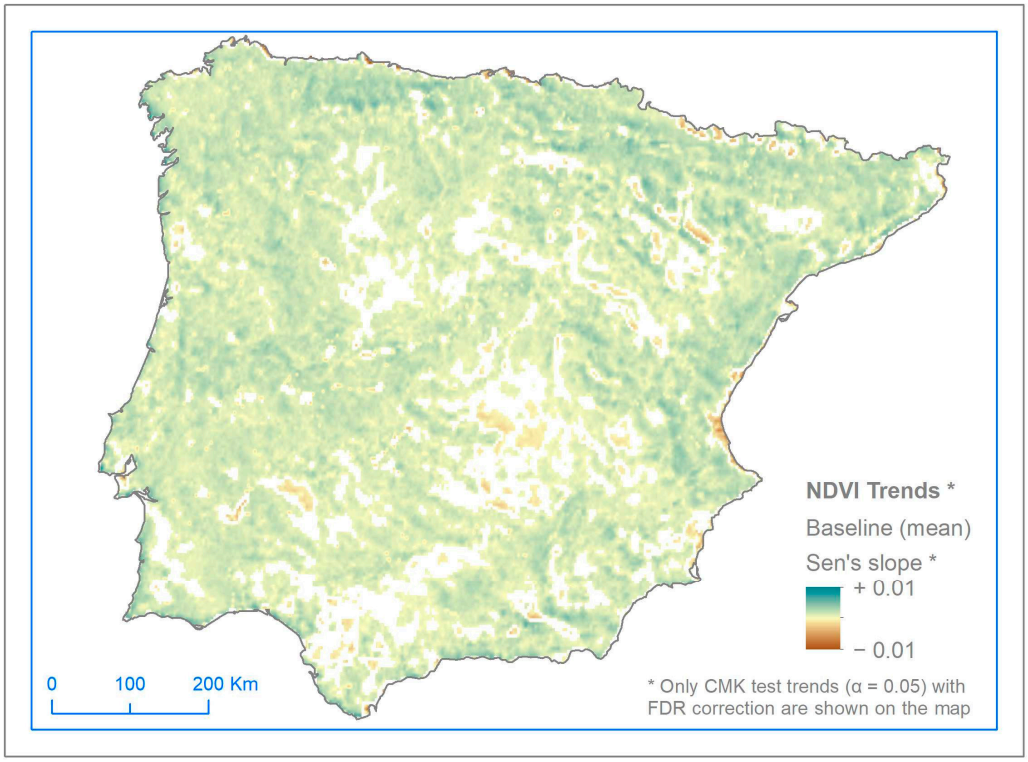

Figure 4. NDVI baseline (Amplitude 0: Annual mean) trends in the Iberian Peninsula (1982–2023). Note: Only the NDVI trends that were statistically significant (α = 0.05) using the CMK test with FDR control are shown on the map. Source: Figure created by the authors.

Figure 6 represents the fitted seasonal curves derived from the entire time series (1982–2023), with each curve representing the modelled phenological data for specific ecoregions. Only pixels with statistically significant trends are represented, ensuring the robustness and reliability of the visualised seasonal patterns. Rather than using data from individual years, such as 1982 and 2023, these curves are based on trends captured across the entire 42-year period, highlighting long-term trends in seasonality.

The long-term trend in the Atlantic ecoregion showed increased NDVI values from 1982 to 2023. The seasonal pattern revealed that NDVI peaked during the summer (July), with values ranging from 0.46 to 0.54. NDVI values started increasing in January, ranging from 0.27 (1982) to 0.35 (2023), and decreased to lower values in December, ranging from 0.25 (1982) to 0.35 (2023). This pattern indicates that the growing season has advanced, with earlier increases in NDVI values compared to previous decades.

We found a more extended period of vegetation growth in the High Mountain areas within the Atlantic ecoregion. The NDVI values increased earlier and peaked in July, starting at 0.43 in 1982 and reaching 0.54 in 2023. The growth period was sustained longer than in other regions, with high values persisting into August. This suggests an advancement in the growing season, with vegetation growth beginning earlier in the year.

In the Mediterranean ecoregion, the long-term trend also indicated a positive increase in NDVI values from 1982 to 2023. This trend was characterised by enhanced vegetation growth and activity throughout the year. The seasonal pattern showed that the NDVI also peaked in the summer, but started at a lower base in January, with values ranging from 0.18 (1982) to 0.26 (2023), and peaked earlier in April, with values between 0.33 and 0.37. The NDVI values then steadily declined until December. This indicates a shift toward earlier seasonal growth, with the NDVI values rising earlier in the year than previously observed.

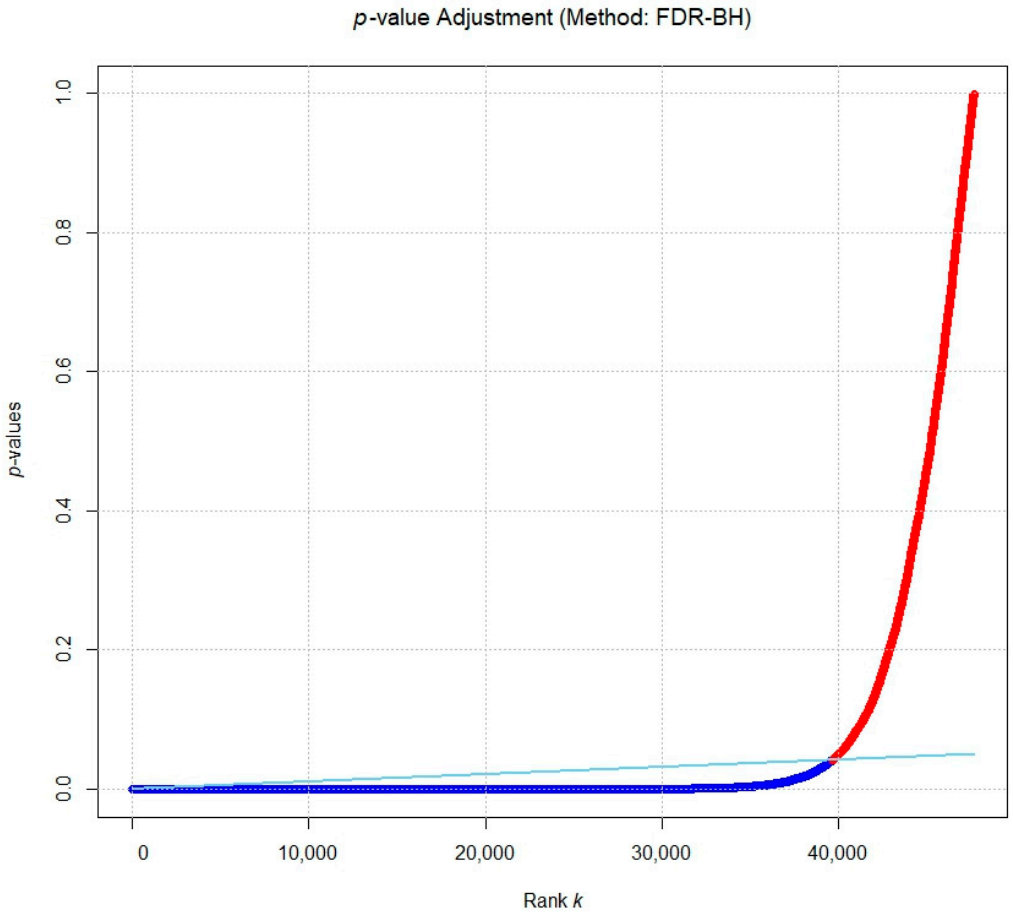

Figure 5. Controlling the false discovery rate (FDR) of annual mean NDVI trends in the Iberian Peninsula (1982–2023) using FDR-BH *p*-value adjustment and the CMK test. Note: The *x*-axis represents the rank (k) of 47,635 *p*-values sorted in ascending order, whilst the *y*-axis displays the observed *p*-values. The celestial blue line symbolises the threshold defined by the FDR, which is calculated using the following expression: $\frac{k \cdot \alpha}{m}$; herein, k denotes the rank, α the significance level, and m the total number of tests conducted. The line coloured in blue indicates the *p*-values that are deemed significant following the application of the FDR control, using the Benjamini–Hochberg method (FDR-BH). Conversely, the line coloured in red represents the *p*-values that are not considered significant according to this adjustment. This bi-coloured line comprises 47,635 points, corresponding to the number of tests performed (m). Source: Figure created by the authors.

In the High Mountain areas within the Mediterranean ecoregion, the long-term trend showed a notable positive trend in vegetation growth from 1982 to 2023. The NDVI values increased, indicating a robust enhancement in vegetation activity over the period. The seasonal pattern showed that the NDVI values began to rise in February and peaked in June, with values ranging from 0.36 (1982) to 0.43 (2023), followed by a decrease towards the end of the year. This region revealed a more pronounced mid-year peak compared to the other areas. The shift towards earlier peaks indicates a change in the timing of the growing season, with the NDVI values rising earlier in the year.

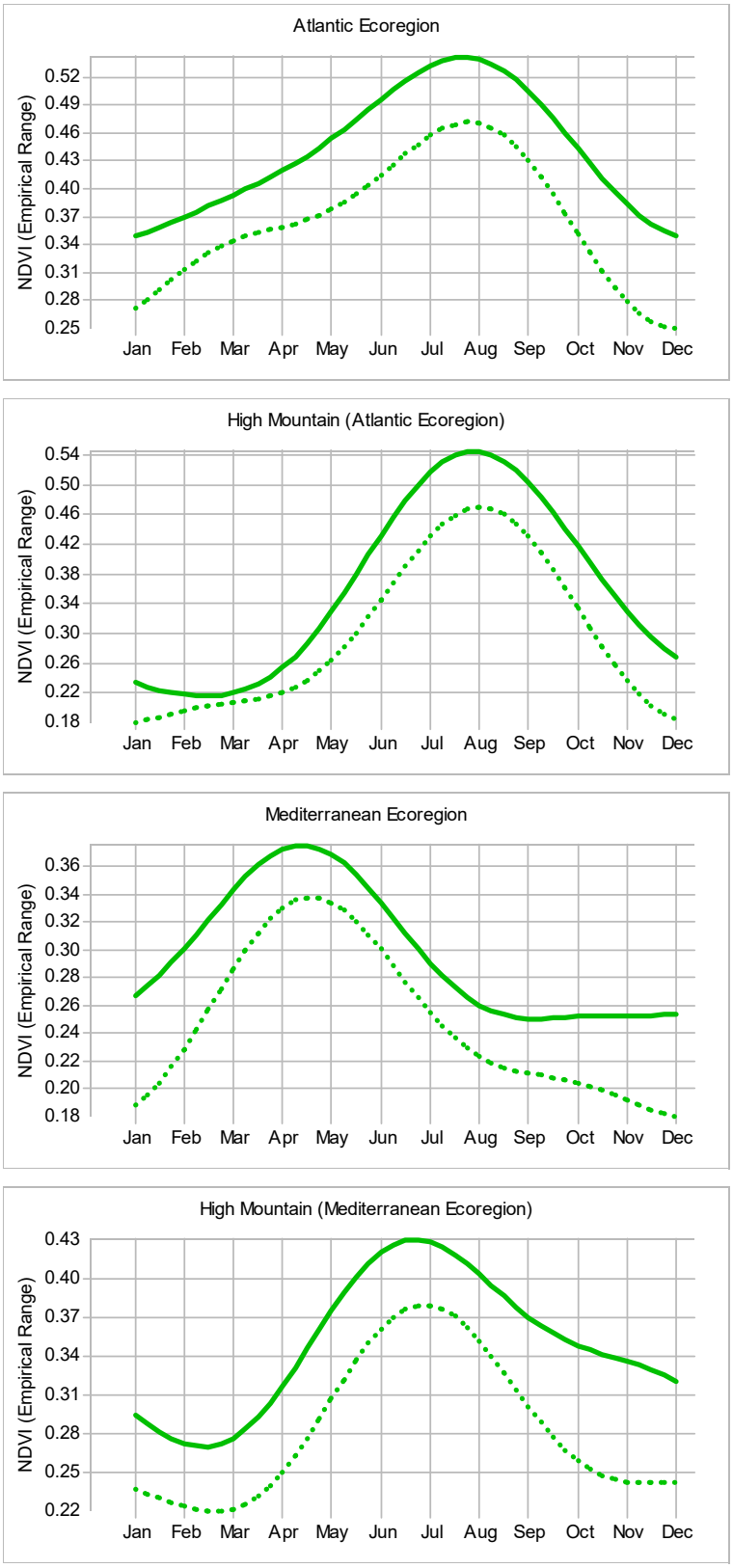

Figure 6. Fitted seasonal curves (1982–2023). Note: These curves do not represent specific years, but are generalised abstractions of long-term trends derived from the entire dataset. The green dashed line represents the trend for the first year (1982), while the green continuous line represents the trend for the last year of the series (2023). Source: Figure created by the authors.

The Atlantic ecoregion consistently showed the highest average NDVI values, peaking at 0.54 in July due to its dense vegetation and favourable climatic conditions. The High Mountain areas in the Atlantic ecoregion experienced the greatest long-term increase in NDVI values from 1982 to 2023, reflecting a strong positive trend in vegetation cover and significant enhancement in vegetation activity over the decades. The Mediterranean ecoregion showed the largest seasonal changes, with NDVI values peaking earlier around April (0.37) and steadily declining through the summer, indicating significant variability and adaptation to changing climatic conditions. Overall, all ecoregions proved a positive trend in NDVI from 1982 to 2023, suggesting increased vegetation activity and advancements in the growing season.

Across the Atlantic and Mediterranean ecoregions, a general increase in NDVI values was observed over the study period, indicating an overall positive trend in vegetation activity. This increase was consistent across all regions, with earlier rises in NDVI values suggesting a shift towards earlier growing seasons. In both ecoregions, the NDVI values reached their highest levels during the summer months, although the timing of these peaks varied between regions.

The main differences between the ecoregions were observed in the timing and duration of the NDVI peaks. In the Atlantic ecoregion, the NDVI values remained high for extended periods, particularly in the High Mountain areas, where elevated values persisted longer into the growing season. In contrast, in the Mediterranean ecoregion, the growing season started earlier, with a sharper increase and an earlier peak, followed by a steady decline through the summer. Additionally, the lowest baseline NDVI values at the beginning of the growing season were observed in the High Mountain areas of the Atlantic ecoregion, while the most significant increases in the NDVI values over the study period occurred in the High Mountain areas of the Mediterranean ecoregion. The underlying factors contributing to these observed differences will be further analysed in the discussion section.

4. Discussion

This research analysed vegetation seasonality trends in the Iberian Peninsula from 1982 to 2023 using the spatiotemporal time series of AVHRR NDVI data. Our seasonal trend analysis revealed significant spatial trends in the phenological parameters in the Iberian Peninsula. The findings indicate a widespread increase in vegetation activity, reflecting a generalised greening process over the forty-four-year period. These significant trends underscore substantial shifts in the timing and intensity of vegetation growth, with the growing season beginning earlier each year.

Several key methodological strengths highlight the robustness of our seasonal trend analysis with false discovery rate control. Firstly, the extensive data series length from 1982 to 2023 provides a comprehensive long-term perspective of NDVI trends. Additionally, the temporal frequency of the data ensures detailed monitoring of seasonal fluctuations, enhancing the resolution of our trend detection. Complete geographic coverage of the Iberian Peninsula ensures that the analysis represents diverse ecological zones. Statistically, the robustness of our approach is further reinforced by using the CMK test combined with the FDR control. The original seasonal trend analysis (STA) methodology does not include the CMK test, and the FDR control is an additional innovation, further strengthening the statistical reliability of the detected trends [64]. This innovative incorporation of FDR correction into our seasonal trend analysis uniquely addresses the multiple testing problem [65], significantly reducing the chances of Type I errors and increasing the reliability of our findings [66,67].

Our analysis of interannual trends confirmed a dominant greening trend in the Iberian Peninsula, aligning with other studies conducted independently in Spain and Portugal [68–73], and reflecting the broader pattern of global greening [74]. Vicente-Serrano et al. (2020) [68] analysed the time series (1981–2015) of AVHRR NDVI data and found a clear positive NDVI trend in approximately 80% of mainland Spain and the Balearic Islands. In our research, covering the period from 1982 to 2023, we observed significant greening

trends across 83.16% of the Iberian Peninsula. Notably, we adopted a more stringent approach to statistical significance by combining the CMK test with the TS slope estimator, and we applied the FDR control, enhancing our findings' statistical reliability by controlling for multiple testing.

One of the most significant findings was that we observed approximately 94.2% of the Iberian Peninsula experiencing a significant trend in at least one of the seasonality parameters for the period 1982–2023. These trends included consistent increases in the NDVI baseline across all seasons, an earlier start of the growing season, greening onset, and shifts in the timing of the senescence period. Several authors have reported that the greening period starts earlier, and the senescence period lengthens, which others have linked to rising temperatures [75,76]. The earlier green-up is seen because of increased temperatures [77]. This also leads to a longer growing season, associated with increased carbon sequestration [61] and exposes vegetation to greater potential drought stress [78]. The earlier peak and decline in NDVI values in the Mediterranean ecoregion suggest increased wildfire risk during summer, necessitating improved fire management strategies [79,80]. Adell-Michavila et al. (2024) [81] also reported changes in phenological trends in Spain during the period 1983–2020, noting significant contrasts among land covers. Caparrós et al. (2020) [82] analysed vegetation phenology in the Iberian Peninsula and the Balearic Islands from 2001 to 2017 using MODIS reflectance data. Their results revealed distinct differences between the Atlantic and Mediterranean ecoregions in the spring and autumn phenophases. Additionally, the phenological behaviour in the Mediterranean mountainous ecoregion was like that of the Atlantic vegetation [83,84]. We identified distinct phenological patterns for each ecoregion, including a unique pattern in the high mountain areas of the Mediterranean ecoregion, combining characteristics of both Mediterranean and Atlantic regions.

Despite our research's comprehensive scope and robust methodology, several limitations should be acknowledged. Firstly, relying on satellite-based NDVI data may not fully capture fine-scale phenological variations due to its relatively coarse spatial resolution. However, we opted for a high temporal resolution and a generalised approach, allowing us to capture long-term seasonal trends accurately. This approach prioritises the frequency of observations over spatial detail, aligning with our goal of exploring the effects of global change at ecoregional scales. Additionally, the analysis does not fully account for the potential influence of non-climatic factors, such as land use changes and management practices, which could also impact vegetation dynamics. This limitation could be addressed by applying the methodology at the level of land cover classes and, even more specifically, at the level of vegetation formations with predominant species, as has already been carried out with the Spanish fir forests [84]. Using other vegetation indices, such as the enhanced vegetation index (EVI) [85], could provide complementary insights and improve the detection of subtle trends. This would be particularly useful in capturing shallow and high values of vegetation activity. Moreover, integrating multiple time series datasets could offer a more nuanced understanding of long-term trends and drivers. It would also be interesting to compare the same indicators (NDVI, EVI) across different sensors (AVHRR, MODIS), which would provide an opportunity to validate the results. However, addressing these limitations would require a focused and comprehensive investigation dedicated exclusively to this purpose. This will serve as a key component of our future research roadmap.

5. Conclusions

Over the past four decades, significant trends in vegetation seasonality and greening have been identified across the Iberian Peninsula, reflecting enhanced vegetation activity and a general adaptation to climate change. These trends point to earlier growing seasons and extended growth periods, which carry important implications for land management.

The phenological shifts observed highlight the need for adaptive land-use strategies that consider these changes in growing seasons. Sustainable agricultural practices must evolve to address altered water availability and potential impacts on crop productivity. Op-

timising water resources and adjusting farming practices to align with shifting phenological patterns will be crucial, particularly in vulnerable regions like the Mediterranean. However, it is essential to recognise that the observed greening cannot continue indefinitely and may eventually lead to ecosystem collapse, with increased risks of forest fires and water stress. Conservation efforts should also focus on preserving biodiversity, as changes in vegetation cycles can disrupt species interactions. Long-term studies like this one provide valuable data to guide regional-scale management decisions, ensuring the sustainable use of natural resources in the face of ongoing climate change.

Future research should explore variations in phenological responses across different regions, land cover types, and the effects of extreme weather events. Integrating high-resolution remote sensing with ground-based observations will provide a deeper understanding of vegetation dynamics. Additionally, there is a need for rigorous statistical methods to address multiple testing challenges and ensure the reliability of the findings.

Our results revealed significant seasonality trends that align with observed climate trends, supporting the hypothesis that climate change alters vegetation seasonality patterns. This underscores the importance of satellite-based remote sensing for monitoring ecological responses to global change and meeting the study's objectives.

Author Contributions: Conceptualisation: O.G.-H.; methods: O.G.-H. and L.V.G.; software: O.G.-H.; formal analysis: O.G.-H. and L.V.G.; investigation: O.G.-H. and L.V.G.; writing—original draft preparation: O.G.-H.; writing—review and editing: O.G.-H. and L.V.G. All authors have read and agreed to the published version of the manuscript.

Funding: This research received no external funding.

Institutional Review Board Statement: Not applicable.

Informed Consent Statement: Not applicable.

Data Availability Statement: The complete dataset supporting this study's findings is available from the corresponding author, O.G.-H.

Acknowledgments: This investigation contributes to the projects of PALEONIEVES (ref. 3025/2023) and PALEOPINSAPO II (ref. PID2022-141592NB-I00). We sincerely thank the reviewers for their valuable contributions in improving the original manuscript. We also thank the editorial team for their insightful suggestions and meticulous corrections, which have greatly improved the quality of the manuscript. We also appreciate the editorial team for waiving the publication fee.

Conflicts of Interest: The authors declare no conflicts of interest.

References

1. Richardson, A.D.; Keenan, T.F.; Migliavacca, M.; Ryu, Y.; Sonnentag, O.; Toomey, M. Climate Change, Phenology, and Phenological Control of Vegetation Feedbacks to the Climate System. *Agric. For. Meteorol.* **2013**, *169*, 156–173. [CrossRef]
2. Ma, S.; Pitman, A.J.; Lorenz, R.; Kala, J.; Srbinovsky, J. Earlier Green-up Amplifies Spring Warming over Europe. *Geophys. Res. Lett.* **2016**, *46*, 582–589. [CrossRef]
3. Westerling, A.L.; Hidalgo, H.G.; Cayan, D.R.; Swetnam, T.W. Warming and Earlier Spring Increase Western U.S. Forest Wildfire Activity. *Science* **2006**, *313*, 940–943. [CrossRef] [PubMed]
4. Liu, Q.; Piao, S.; Fu, Y.H.; Gao, M.; Peñuelas, J.; Janssens, I.A. Climatic Warming Increases Spatial Synchrony in Spring Vegetation Phenology Across the Northern Hemisphere. *Geophys. Res. Lett.* **2019**, *46*, 1641–1650. [CrossRef]
5. Wu, C.; Wang, X.; Wang, H.; Ciais, P.; Peñuelas, J.; Myneni, R.B.; Desai, A.R.; Gough, C.M.; Gonsamo, A.; Black, A.T.; et al. Contrasting Responses of Autumn-Leaf Senescence to Daytime and Night-Time Warming. *Nat. Clim. Chang.* **2018**, *8*, 1092–1096. [CrossRef]
6. Xie, Y.; Wang, X.; Silander, J.A. Deciduous Forest Responses to Temperature, Precipitation, and Drought Imply Complex Climate Change Impacts. *Proc. Natl. Acad. Sci. USA* **2015**, *112*, 13585–13590. [CrossRef]
7. Ma, X.; Zhu, X.; Xie, Q.; Jin, J.; Zhou, Y.; Luo, Y.; Liu, Y.; Tian, J.; Zhao, Y. Monitoring Nature's Calendar from Space: Emerging Topics in Land Surface Phenology and Associated Opportunities for Science Applications. *Glob. Chang. Biol.* **2022**, *28*, 7186–7204. [CrossRef]
8. Moss, S. *A Bird in the Bush: A Social History of Birdwatching*; Aurum Press: London, UK, 2004.
9. Lawrence, A. The First Cuckoo in Winter: Phenology, Recording, Credibility and Meaning in Britain. *Glob. Environ. Change* **2009**, *19*, 173–179. [CrossRef]

10. Kuenzer, C.; Dech, S.; Wagner, W. (Eds.) *Remote Sensing Time Series*; Springer International Publishing: Cham, Switzerland, 2015; Volume 22, ISBN 978-3-319-15966-9.
11. Purkis, S.; Klemas, V. *Remote Sensing and Global Environmental Change*; Wiley-Blackwell: Hoboken, NJ, USA, 2011.
12. Jones, H.G.; Vaughan, R.A. *Remote Sensing of Vegetation: Principles, Techniques, and Applications*; OUP Oxford: New York, NY, USA, 2010.
13. Kuenzer, C.; Dech, S.; Wagner, W. *Remote Sensing Time Series Revealing Land Surface Dynamics: Status Quo and the Pathway Ahead*; Springer: Berlin/Heidelberg, Germany, 2015; pp. 1–24.
14. Schwartz, M.D. *Phenology: An Integrative Environmental Science*; Schwartz, M.D., Ed.; Springer: Dordrecht, The Netherlands, 2013; ISBN 978-94-007-6924-3.
15. Helman, D. Land Surface Phenology: What Do We Really 'See' from Space? *Sci. Total Environ.* **2018**, *618*, 665–673. [CrossRef]
16. Reed, B.C.; Schwartz, M.D.; Xiao, X. Remote Sensing Phenology. In *Phenology: An Integrative Environmental Science*; Springer: Berlin/Heidelberg, Germany, 2009; Volume 39, pp. 231–246. [CrossRef]
17. Lieth, H. (Ed.) *Phenology and Seasonality Modeling*; Springer: Berlin/Heidelberg, Germany, 1974; Volume 8, ISBN 978-3-642-51865-2.
18. Zeng, L.; Wardlow, B.D.; Xiang, D.; Hu, S.; Li, D. A Review of Vegetation Phenological Metrics Extraction Using Time-Series, Multispectral Satellite Data. *Remote Sens. Environ.* **2020**, *237*, 111511. [CrossRef]
19. Chmielewski, F.-M. Phenology in Agriculture and Horticulture. In *Phenology: An Integrative Environmental Science*; Springer: Dordrecht, The Netherlands, 2013; pp. 539–561.
20. Frank, J.H.; Frank, J.H.; Thomas, M.C.; Yousten, A.A.; Howard, F.W.; Giblin-davis, R.M.; Heppner, J.B.; Zuparko, R.L.; Sánchez, N.E.; Luna, M.G.; et al. Phenology Models for Pest Management. In *Encyclopedia of Entomology*; Springer: Dordrecht, The Netherlands, 2008; pp. 2834–2841.
21. Chuine, I. Why Does Phenology Drive Species Distribution? *Philos. Trans. R. Soc. B Biol. Sci.* **2010**, *365*, 3149–3160. [CrossRef] [PubMed]
22. Jonsson, P.; Eklundh, L. Seasonality Extraction by Function Fitting to Time-Series of Satellite Sensor Data. *IEEE Trans. Geosci. Remote Sens.* **2002**, *40*, 1824–1832. [CrossRef]
23. Duarte, L.; Teodoro, A.C.; Monteiro, A.T.; Cunha, M.; Gonçalves, H. QPhenoMetrics: An Open Source Software Application to Assess Vegetation Phenology Metrics. *Comput. Electron. Agric.* **2018**, *148*, 82–94. [CrossRef]
24. Verger, A.; Filella, I.; Baret, F.; Peñuelas, J. Vegetation Baseline Phenology from Kilometric Global LAI Satellite Products. *Remote Sens. Environ.* **2016**, *178*, 1–14. [CrossRef]
25. Zhang, X.; Friedl, M.A.; Schaaf, C.B.; Strahler, A.H.; Hodges, J.C.F.; Gao, F.; Reed, B.C.; Huete, A. Monitoring Vegetation Phenology Using MODIS. *Remote Sens. Environ.* **2003**, *84*, 471–475. [CrossRef]
26. Younes, N.; Joyce, K.E.; Maier, S.W. All Models of Satellite-Derived Phenology Are Wrong, but Some Are Useful: A Case Study from Northern Australia. *Int. J. Appl. Earth Obs. Geoinf.* **2021**, *97*, 102285. [CrossRef]
27. Eastman, J.R.; Sangermano, F.; Ghimire, B.; Zhu, H.; Chen, H.; Neeti, N.; Cai, Y.; Machado, E.A.; Crema, S.C. Seasonal Trend Analysis of Image Time Series. *Int. J. Remote Sens.* **2009**, *30*, 2721–2726. [CrossRef]
28. Roerink, G.J.; Menenti, M.; Soepboer, W.; Su, Z. Assessment of Climate Impact on Vegetation Dynamics by Using Remote Sensing. *Phys. Chem. Earth* **2003**, *28*, 103–109. [CrossRef]
29. Huang, S.; Tang, L.; Hupy, J.P.; Wang, Y.; Shao, G. A Commentary Review on the Use of Normalized Difference Vegetation Index (NDVI) in the Era of Popular Remote Sensing. *J. Res.* **2021**, *32*, 2719. [CrossRef]
30. Eamus, D.; Huete, A.; Yu, Q. *Vegetation Dynamics. A Synthesis of Plant Ecophysiology, Remote Sensing and Modelling*; Cambridge University Press: Cambridge, UK, 2016; ISBN 9781107286221.
31. Pettorelli, N.; Vik, J.O.; Mysterud, A.; Gaillard, J.M.; Tucker, C.J.; Stenseth, N.C. Using the Satellite-Derived NDVI to Assess Ecological Responses to Environmental Change. *Trends Ecol. Evol.* **2005**, *20*, 503–510. [CrossRef]
32. Clarivate Analytics. *Research Fronts 2020*; Clarivate Analytics: London, UK, 2021.
33. Aurelle, D.; Thomas, S.; Albert, C.; Bally, M.; Bondeau, A.; Boudouresque, C.; Cahill, A.E.; Carlotti, F.; Chenuil, A.; Cramer, W.; et al. Biodiversity, Climate Change, and Adaptation in the Mediterranean. *Ecosphere* **2022**, *13*, 3915. [CrossRef]
34. Urdiales-Flores, D.; Zittis, G.; Hadjinicolaou, P.; Osipov, S.; Klingmüller, K.; Mihalopoulos, N.; Kanakidou, M.; Economou, T.; Lelieveld, J. Drivers of Accelerated Warming in Mediterranean Climate-Type Regions. *NPJ Clim. Atmos. Sci.* **2023**, *6*, 97. [CrossRef]
35. Tapiador, F.J. *The Geography of Spain*; World Regional Geography Book Series; Springer International Publishing: Cham, Switzerland, 2020; ISBN 978-3-030-18906-8.
36. Vieira, G.; Zêzere, J.L.; Mora, C. (Eds.) *Landscapes and Landforms of Portugal*; Springer International Publishing: Cham, Switzerland, 2020; ISBN 978-3-319-03640-3.
37. Olson, D.M.; Dinerstein, E.; Wikramanayake, E.D.; Burgess, N.D.; Powell, G.V.N.; Underwood, E.C.; D'amico, J.A.; Itoua, I.; Strand, H.E.; Morrison, J.C.; et al. Terrestrial Ecoregions of the World: A New Map of Life on EarthA New Global Map of Terrestrial Ecoregions Provides an Innovative Tool for Conserving Biodiversity. *Bioscience* **2001**, *51*, 933–938. [CrossRef]
38. Kottek, M.; Grieser, J.; Beck, C.; Rudolf, B.; Rubel, F. World Map of Köppen−Geiger Climate Classification. *Meteorol. Z.* **2006**, *15*, 259–263. [CrossRef] [PubMed]
39. JRC. *The Digital Observatory for Protected Areas (DOPA) Explorer 3.1: Cantabrian Mixed Forests*; Joint Research Centre—European Commission: Brussels, Belgium, 2019.
40. Jacques, B.; Aronson, J. *Biology and Wildlife of the Mediterranean*; Oxford University Press: Oxford, UK, 1999.

41. Gutiérrez-Hernández, O.; Senciales-González, J.M.; García, L. V Evolución de La Superficie Forestal En Andalucía. Procesos y Factores. *Rev. Estud. Andal.* **2016**, *33*, 111–148. [CrossRef]
42. García-Ruiz, J.M.; Arnáez, J.; Lasanta, T.; Nadal-Romero, E.; López-Moreno, J.I. The Climate of the Mountains, Originality and Spatial Variability. In *Mountain Environments: Changes and Impacts*; Earth and Environmental Sciences Library; Springer: Cham Switzerland, 2024; pp. 95–116. [CrossRef]
43. Chazarra Bernabé, A.; Lorenzo Mariño, B.; Romero Fresneda, R.; Moreno García, J.V. *Evolución de Los Climas de Köppen En España En El Periodo 1951–2020*; Agencia Estatal de Meteorologa. Ministerio para la Tranísición Ecológica y el Reto Demográfico; Gobierno de España: Madrid, Spain, 2022.
44. NOAA. AVHRR NDVI Data from the Vegetation Health Products. 2024. Available online: https://www.star.nesdis.noaa.gov/smcd/emb/vci/VH/vh_ftp.php (accessed on 31 July 2024).
45. Kogan, F.; Vargas, M.; Guo, W. Comparison of AVHRR-Based Global Data Records. In *NATO Science for Peace and Security Series C: Environmental Security*; Springer Nature: Berlin/Heidelberg, Germany, 2011; pp. 267–272.
46. Latifovic, R.; Pouliot, D.; Dillabaugh, C. Identification and Correction of Systematic Error in NOAA AVHRR Long-Term Satellite Data Record. *Remote Sens. Environ.* **2012**, *127*, 84–97. [CrossRef]
47. Gutman, G.; Masek, J.G. Long-Term Time Series of the Earth's Land-Surface Observations from Space. *Int. J. Remote Sens.* **2012**, *33*, 4700–4719. [CrossRef]
48. Holben, B.N. Characteristics of Maximum-Value Composite Images from Temporal AVHRR Data. *Int. J. Remote Sens.* **1986**, *7*, 1417–1434. [CrossRef]
49. Roerink, G.J.; Menenti, M.; Verhoef, W. Reconstructing Cloudfree NDVI Composites Using Fourier Analysis of Time Series. *Int. J. Remote Sens.* **2000**, *21*, 1911–1917. [CrossRef]
50. NOAA. *NOAA Blended Vegetation Health Product (Blended-VHP) 2018*; National Oceanic and Atmospheric Administration (NOAA): Silver Spring, MD, USA, 2018.
51. Heumann, B.W. The Multiple Comparison Problem in Empirical Remote Sensing. *Photogramm. Eng. Remote Sens.* **2015**, *81*, 921–926. [CrossRef]
52. Eastman, J. *ClarkLabs Earth Trends Modeler in TerrSet 2020*; Clark University: Worcester, MA, USA, 2021.
53. Colquhoun, D. An Investigation of the False Discovery Rate and the Misinterpretation of *p*-Values. *R. Soc. Open Sci.* **2014**, *1*, 140216. [CrossRef] [PubMed]
54. Eastman, J. *ClarkLabs TerrSet: Geospatial Monitoring and Modeling Software, Version 19.08.2023*; Clark University: Worcester, MA, USA, 2023.
55. Theil, H. *A Rank-Invariant Method of Linear and Polynomial Regression Analysis I, II and III*; Section of Sciences, Koninklijke Academie van Wetenschappen te: Amsterdam, The Netherlands, 1950; pp. 386–392.
56. Sen, P. Estimates of the Regression Coefficient Based on Kendall's Tau. *J. Ofthe Am. Stat. Assoc.* **1968**, *63*, 1379–1389. [CrossRef]
57. Neeti, N.; Eastman, J.R. A Contextual Mann-Kendall Approach for the Assessment of Trend Significance in Image Time Series. *Trans. GIS* **2011**, *15*, 599–611. [CrossRef]
58. Mann, H. Nonparametric Tests against Trend. *Econometrica* **1945**, *13*, 245–259. [CrossRef]
59. Kendall, M. *Rank Correlation Methods*; Charles Griffin: London, UK, 1975.
60. Hoaglin, D.; Mosteller, F.; Tukey, J. *Understanding Robust and Exploratory Data Analysis*; John Wiley and Sons: New York, NY, USA, 2000.
61. Efron, B. *Large-Scale Inference*; Cambridge University Press: Cambridge, UK, 2010. [CrossRef]
62. Benjamini, Y.; Hochberg, Y. Controlling the False Discovery Rate: A Practical and Powerful Approach to Multiple Testing. *J. R. Stat. Soc. Ser. B* **1995**, *57*, 89–300. [CrossRef]
63. Eastman, J. ClarkLabs. In *TerrSet: Geospatial Monitoring and Modeling—Tutorial*; Clark University: Worcester, MA, USA, 2016.
64. Gutiérrez-Hernández, O.; García, L.V. Robust Trend Analysis in Environmental Remote Sensing: A Case Study of Cork Oak Forest Decline. *Remote Sens.* **2024**, *16*, 3886. [CrossRef]
65. Gutiérrez Hernández, O.; García, L. Multiple Testing in Remote Sensing: Addressing the Elephant in the Room. *SSRN* **2024**, 4891512. [CrossRef]
66. García, L.V. Escaping the Bonferroni Iron Claw in Ecological Studies. *Oikos* **2004**, *105*, 657–663. [CrossRef]
67. García, L.V. Controlling the False Discovery Rate in Ecological Research. *Trends Ecol. Evol.* **2003**, *18*, 553–554. [CrossRef]
68. Vicente-Serrano, S.M.; Martín-Hernández, N.; Reig, F.; Azorin-Molina, C.; Zabalza, J.; Beguería, S.; Domínguez-Castro, F.; El Kenawy, A.; Peña-Gallardo, M.; Noguera, I.; et al. Vegetation Greening in Spain Detected from Long Term Data (1981–2015). *Int. J. Remote Sens.* **2020**, *41*, 1709–1740. [CrossRef]
69. Gutiérrez Hernández, O. Tendencias Recientes Del NDVI En Andalucía: Los Límites Del Reverdecimiento. *Bol. Asoc. Geógr. Español.* **2022**, *94*. [CrossRef]
70. Costa, R.; Fraga, H.; Fernandes, P.; Santos, J. Climate-Driven Variability in Vegetation Greenness over Portugal. *Clim. Res.* **2018**, *76*, 95–113. [CrossRef]
71. Novillo, C.J.; Arrogante-Funes, P.; Romero-Calcerrada, R. Recent NDVI Trends in Mainland Spain: Land-Cover and Phytoclimatic-Type Implications. *ISPRS Int. J. Geoinf.* **2019**, *8*, 43. [CrossRef]
72. Alcaraz-Segura, D.; Liras, E.; Tabik, S.; Paruelo, J.; Cabello, J. Evaluating the Consistency of the 1982-1999 NDVI Trends in the Iberian Peninsula across Four Time-Series Derived from the AVHRR Sensor: LTDR, GIMMS, FASIR, and PAL-II. *Sensors* **2010**, *10*, 1291–1314. [CrossRef]

73. del Barrio, G.; Puigdefabregas, J.; Sanjuan, M.E.; Stellmes, M.; Ruiz, A. Assessment and Monitoring of Land Condition in the Iberian Peninsula, 1989-2000. *Remote Sens. Environ.* **2010**, *114*, 1817–1832. [CrossRef]
74. Gutiérrez-Hernández, O.; García, L.V. Uncovering True Significant Trends in Global Greening. *Remote Sens. Appl.* **2024**, 101377. [CrossRef]
75. Badeck, F.W.; Bondeau, A.; Böttcher, K.; Doktor, D.; Lucht, W.; Schaber, J.; Sitch, S. Responses of Spring Phenology to Climate Change. *New Phytol.* **2004**, *162*, 295–309. [CrossRef]
76. Wang, X.; Wu, C. Estimating the Peak of Growing Season (POS) of China's Terrestrial Ecosystems. *Agric. Meteorol.* **2019**, *278*, 107639. [CrossRef]
77. Shen, M.; Zhu, X.; Peng, D.; Jiang, N.; Huang, Y.; Chen, J.; Wang, C.; Zhao, W. Greater Temperature Sensitivity of Vegetation Greenup Onset Date in Areas with Weaker Temperature Seasonality across the Northern Hemisphere. *Agric. Meteorol.* **2022**, *313*, 108759. [CrossRef]
78. Zhang, K.; Kimball, J.S.; Mu, Q.; Jones, L.A.; Goetz, S.J.; Running, S.W. Satellite Based Analysis of Northern ET Trends and Associated Changes in the Regional Water Balance from 1983 to 2005. *J. Hydrol.* **2009**, *379*, 92–110. [CrossRef]
79. Resco de Dios, V.; Fischer, C.; Colinas, C. Climate Change Effects on Mediterranean Forests and Preventive Measures. *New For.* **2006**, *33*, 29–40. [CrossRef]
80. Resco de Dios, V.; Cunill Camprubí, À.; Pérez-Zanón, N.; Peña, J.C.; Martínez del Castillo, E.; Rodrigues, M.; Yao, Y.; Yebra, M.; Vega-García, C.; Boer, M.M. Convergence in Critical Fuel Moisture and Fire Weather Thresholds Associated with Fire Activity in the Pyroregions of Mediterranean Europe. *Sci. Total Environ.* **2022**, *806*, 151462. [CrossRef] [PubMed]
81. Adell Michavila, M.; Vicente-Serrano, S.M.; Montorio Llovería, R.; Cai, Z.; Eklundh, L. Evaluación Espacialmente Continua de La Dinámica de La Fenología Vegetal En España Entre 1983 y 2020 a Partir de Imágenes de Satélite. *Cuad. Investig. Geográfica* **2024**, *50*, 145–178. [CrossRef]
82. Caparros-Santiago, J.A.; Rodríguez-Galiano, V.F. Estimación de La Fenología de La Vegetación a Partir de Imágenes de Satélite: El Caso de La Península Ibérica e Islas Baleares (2001–2017). *Rev. Teledetección* **2020**, *25*, 13632. [CrossRef]
83. Gutiérrez-Hernández, O. Fenología de Los Ecosistemas de Alta Montaña En Andalucía: Análisis de La Tendencia Estacional Del SAVI (2000–2019). *Pirineos* **2020**, *175*, e055. [CrossRef]
84. Gutiérrez-Hernández, O.; Cámara-Artigas, R.; García, L. V Regeneración de Los Pinsapares Béticos. Análisis de Tendencia Interanual y Estacional Del NDVI. *Pirineos. Rev. Ecol. Montaña* **2018**, *173*, e035. [CrossRef]
85. Huete, A.; Didan, K.; Miura, T.; Rodriguez, E.P.; Gao, X.; Ferreira, L.G. Overview of the Radiometric and Biophysical Performance of the MODIS Vegetation Indices. *Remote Sens. Environ.* **2002**, *83*, 195–213. [CrossRef]